



HAL
open science

Single-Step 3D Printing of Micro-Optics with Adjustable Refractive Index by Ultrafast Laser Nanolithography

D. Gonzalez-Hernandez, B. Sanchez-Padilla, D. Gailevičius, S. Chandran Thodika, S. Juodkazis, Etienne Brasselet, M. Malinauskas

► To cite this version:

D. Gonzalez-Hernandez, B. Sanchez-Padilla, D. Gailevičius, S. Chandran Thodika, S. Juodkazis, et al.. Single-Step 3D Printing of Micro-Optics with Adjustable Refractive Index by Ultrafast Laser Nanolithography. *Advanced Optical Materials*, 2023, 11 (14), 10.1002/adom.202300258 . hal-04293645

HAL Id: hal-04293645

<https://hal.science/hal-04293645v1>

Submitted on 18 Nov 2023

HAL is a multi-disciplinary open access archive for the deposit and dissemination of scientific research documents, whether they are published or not. The documents may come from teaching and research institutions in France or abroad, or from public or private research centers.

L'archive ouverte pluridisciplinaire **HAL**, est destinée au dépôt et à la diffusion de documents scientifiques de niveau recherche, publiés ou non, émanant des établissements d'enseignement et de recherche français ou étrangers, des laboratoires publics ou privés.

Single-Step 3D Printing of Micro-Optics with Adjustable Refractive Index by Ultrafast Laser Nanolithography

D. Gonzalez-Hernandez, B. Sanchez-Padilla, D. Gailevičius, S. Chandran Thodika, S. Juodkazis,* E. Brasselet,* and M. Malinauskas*

Laser exposure defines voxel's dimensions as essential building blocks in direct write 3D nanolithography. However, the exposure conditions not only influence the size of the produced features but also their optical properties. This empowers the realization of an adjustable refractive index out of single material by varying the writing strategy while preserving laser 3D nanolithography's flexibility in geometry and high resolution. Here, the refractive index for the 450–1600 nm spectral range of the micro-optics out of SZ2080 hybrid polymer is systematically studied by applying ray and wave optics approaches followed by optical resolution analysis. It reveals the exact value of the laser-printed components instead of the determination assessed by other techniques measuring thin films or bulky volumes of the investigated substance. The studied micro-lenses are of below 100 μm in dimensions and a clear distinction in their performance on low and high exposure doses is found by analyzing it in all different approaches and validating using different lithography setups. Findings reveal the complexity of the refractive index of the 3D micro-optics which is influenced by the material density and morphology. A route for freedom in 3D printing shape and refractive index can be realized by the technological optimization of delicate exposure control in ultrafast laser nanolithography.

1. Introduction

The field of micro-optics made by Multi-Photon Lithography (MPL)^[1,2] has been significantly growing for more than a decade

D. Gonzalez-Hernandez, D. Gailevičius, M. Malinauskas

Laser Research Center

Physics Faculty

Vilnius University

Saulėtekio 10, Vilnius LT-10223, Lithuania

E-mail: mangirdas.malinauskas@ff.vu.lt

B. Sanchez-Padilla, S. C. Thodika, E. Brasselet

Laboratoire Ondes et Matière d'Aquitaine

CNRS

University of Bordeaux

Talence F-33400, France

E-mail: etienne.brasselet@u-bordeaux.fr

S. Juodkazis

Optical Sciences Centre

Swinburne University of Technology

Melbourne 3122, Australia

E-mail: sjuodkazis@swinburne.edu.au

and has accelerated dramatically over the last five years.^[3] Importantly, it empowers conceptually novel scientific research topics^[4,5] and at the same time is entering industrial applications where the standardization of fabrication and reliable performance protocols are crucial.^[6,7] Though MPL as a technique is becoming recognized as additive manufacturing for high-efficiency advanced micro-optical elements and photonic bonds, which even enables 3D printing of inorganic glass-ceramic materials^[8] suitable for a previously inaccessible range of durable compound micro-optics.^[9] Among recent prominent examples are printing out of black resin^[10] or determining the refractive index (RI) at the millimeter object-scale (yet still not for optical elements of $< 100 \mu\text{m}$ overall dimensions and $\leq 1 \mu\text{m}$ feature sizes).^[11,12] On the one hand, it is obvious that the inherent properties of material and required additives will determine behavior of the final 3D structure at micro- and nano-scales, for example, its mechanical rigidity^[13] or optical

resilience against optical breakdown.^[14] On the other hand, it is known that specific physical properties of a laser-polymerized 3D object will be influenced by the polymerization degree (an axial depth of modification at the focal volume). Namely, mechanical, thermal, as well as optical properties, will depend on the degree of cross-linking.^[15–17] Taking control over it enables 3D printing inside the volume of the already solidified/dried resins, for example, the is a rapidly increasing interest in writing waveguiding free-form structures and photonic bonds.^[18–20] However, up to date the controlled cross-linking has only been exploited for bulky shape (volumetric) structures via refractive index modification inside the resin/resist. Thus, it invites to refer to as (3+1)D writing as was named in the original report.^[19] Such an approach extends the 3D photonic micro-integration to a greater flexibility,^[21] however, not fully empowers the capacity of MPL to create 3D arbitrary architectures down to microscale control. On the other hand, based on it some successful efforts were put into producing cell phantoms for biological applications,^[22] However, there are no reports for the exploitation directly targeting the vast potential of micro-optics. The refractive index which is proportional to the mass density has the potential to be defined in polymers down to the feature size of the polymeric gyration radius, hence, enabling true nanoscale. This is the ultimate resolution for pure polymeric

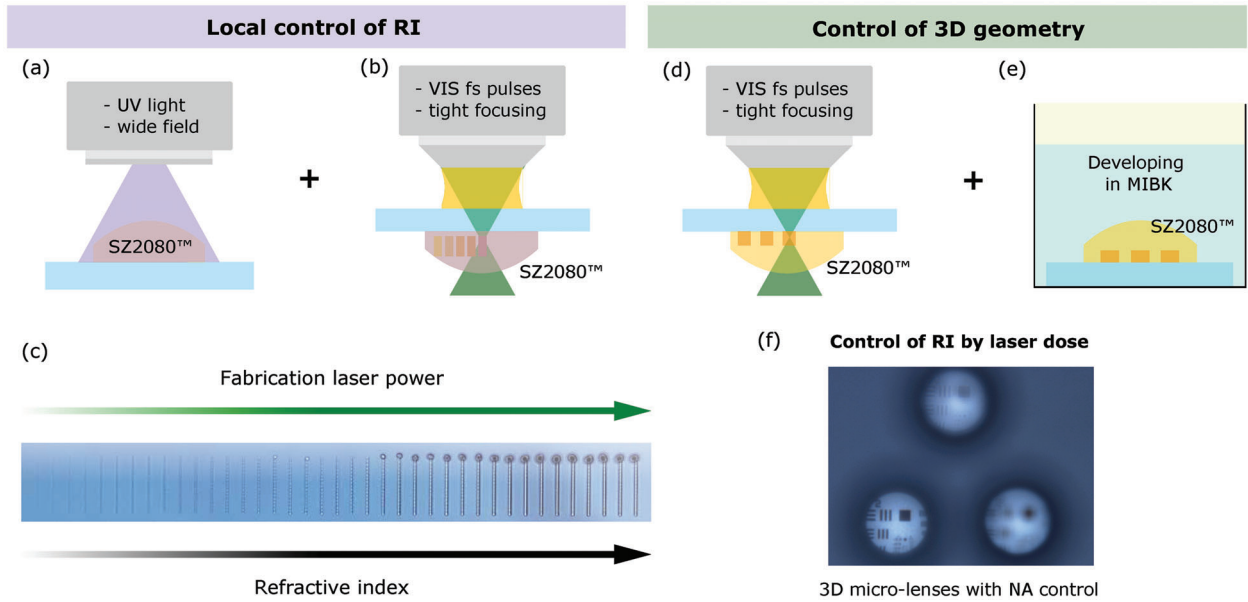


Figure 1. a) OPL setup sketch: UV light for uniform illumination of the droplet of the hybrid organic–inorganic SZ2080 photopolymer. b) MPL setup sketch: femtosecond pulsed laser beam tightly focused into the photopolymer for point-by-point 3D polymerization. c) Optical microscope image of experimental result of combined polymerization. First, OPL followed by a controllable laser writing by MPL. An increase of the polymerization dose is shown by increasingly darker lines. d) MPL setup sketch. e) Development process of MPL polymerized structures in MIBK to wash out the unpolymerized material. f) Optical microscope images of 3D micro-structures via MPL with controlled refractive index by adjusted laser exposure dose, corresponding to different imaging properties of positive 1951 USAF target: magnification, resolving power, and contrast.

materials. Moreover, depending on the molecular structure of the photo-material, natural anisotropy due to its building blocks and corresponding gyration radii could provide limitations or could be used for advantage to engineer anisotropy of refractive index. This is currently unexplored potential. Recently, it was shown that 3D direct laser write can cause residual birefringence in micro-optical elements,^[23] which can be related to residual stresses, polymeric structures, the polarization of writing beam and temperature protocol during laser exposure.

Here, we present a full exploitation of MPL capability to, both, 3D structure and control over the refractive index at a microscale using a widespread hybrid photoresin SZ2080 proven as excellent material for MPL^[24] and optical applications.^[25] This opens a path for creating micro-optical devices with designable refractive index. We validate the exact refractive index of the printed micro-lenses by applying an index matching technique exploiting the immersion in oils of known refractive index. Next to it, we study the distinct behavior of ray and wave optics for elements $< 100 \mu\text{m}$ in dimensions. Such additional control of refractive index enrich the toolbox of 3D printing approaches for refractive and diffractive optics forward programmable 4D printing of materials,^[26] specifically for designable devices dedicated to optical applications.

2. Results

2.1. Laser 3D Nanolithography of Controlled Refractive Index Micro-Optical Components

The refractive index of the photopolymer changes by undergoing through a polymerization process. As a proof of concept, two dif-

ferent polymerization exposure strategies were applied to prove the change of refractive index in the photopolymer SZ2080: ultraviolet (UV) one-photon lithography (OPL) exposure and MPL writing. **Figure 1a** shows the schematic of the UV OPL exposure of a negative-tone photoresist. A droplet of photopolymer is illuminated by a UV radiation until a polymerized state is reached (via accumulation of the required exposure dose). The UV polymerized droplet is then developed following a standard procedure. Via the one-photon exposure, a uniform polymerization degree is reached for the entire material within a solidified droplet. As a second step, MPL writing was applied to the UV pre-polymerized droplet. MPL requires a strongly focused femtosecond (fs-)laser beam with intensity above the material polymerization threshold. The schematic of MPL is shown in **Figure 1b,d**, a high numerical aperture ($NA > 1$, oil immersion) microscope objective lens is used to tightly focus fs-pulses. An oil-immersion technique is applied for MPL writing, where the microscope objective is immersed into oil, which is matching refractive index of the cover glass, through which the photoresist is exposed (**Figure 1b,d**). Laser inscriptions of straight lines at increasing fs-laser intensities shown in **Figure 1c** from left to right. A visible increase of the degree of polymerization in the photopolymer is clearly discernible by a change of optical contrast. The observable optical modification can be achieved by increasing the intensity of fs-pulses (i.e., an average laser power) or by a cumulative exposure at the fixed laser power, but by changing the pulse-to-pulse overlap via laser repetition rate or scan speed / exposure duration. An increasing degree of polymerization was retained after the sample was developed in a chemical bath following the standard procedure as described in **Figure 1e**. The increase in the degree of polymerization has an accumulative effect, which is shown in

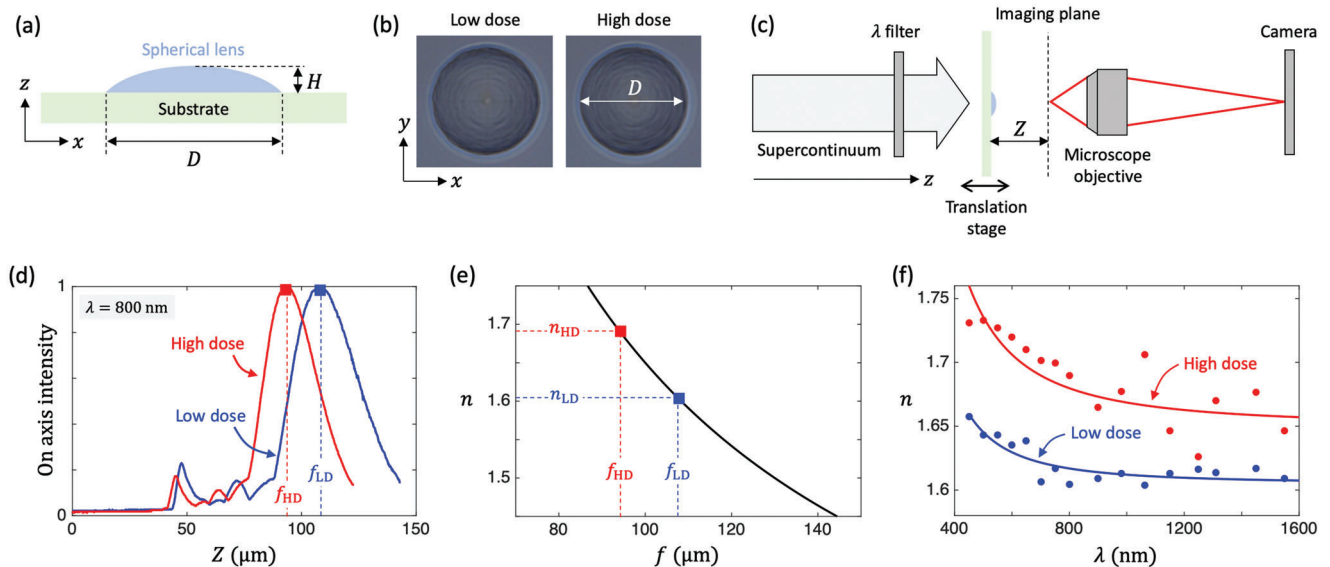


Figure 2. Ray optics approach to the refractive index assessment. a) Sketch of the 3D printed plano-convex spherical lenses with diameter D and height H . b) Microscope images of micro-lenses polymerized at different cumulative doses, $D = 50 \mu\text{m}$, and $H = 5 \mu\text{m}$. c) Setup for the quantitative refractive index assessment via the determination of the focal plane. d) Normalized on-axis intensity distribution along the propagation axis z at 800 nm wavelength for low (blue color) and high (red color) doses, to which we refer to the subscripts LD and HD, respectively. e) Ray optics relationship between the focal length f and the refractive index n . f) Retrieved refractive index dispersion from the visible to the near-infrared domain according to the protocol summarized by panels (d,e). Markers: experimental data. Solid curves: Cauchy fit, see text for details.

this study via its translation into an increase of refractive index by applying the combined dual-curing photopolymerization via steps of one-photon and multi-photon lithographies.

We fabricated spherical micro-lenses by a single exposure of MPL following the presented idea on the observed relation of the refractive index of the micro-structure with the intensity of fs-pulses. Different laser intensities (by changing the laser exposure power corresponding to different exposure doses) were used to create geometrically identical micro-cuboids and micro-lenses out of SZ2080 with two different Laser Direct Writing (LDW) systems (based on commonly used and commercially available laser oscillator and custom made workstation employing laser amplifier), choosing distinct fabrication laser power values (from the dynamic fabrication window^[27]) for Low and High dose following the method in Supporting Information. The difference in refractive index is analyzed by the study of the difference in the focal length of the micro-lenses. Tunability of laser intensity at MPL allowed fabrication of micro-optics with a different controlled refractive index that reflected in their optical performance. It can be observed in Figure 1f, where the contrast of refractive index is seen from 3D micro-optics printed applying variable exposure doses and resulting in different magnification as well as imaging performance of the same test target. Thus, it allows the realization of controlled single-step laser 3D printing of micro-optics with adjustable refractive index independently on the chosen specific laser irradiation source.

2.2. Refractive Index Assessment: Ray Optics Approach

The refractive index of fabricated 3D micro-optics can be determined from the analysis of the optical function of the micro-

optical element itself. For the sake of illustration, this is done for micro-lenses such as those shown in Figure 1f. Namely, we deal with a pair of plano-convex spherical lenses with diameter $D = 50 \mu\text{m}$ and height $H = 5 \mu\text{m}$ labeled as ‘low dose’ and ‘high dose’ recalling the laser polymerization conditions, namely, 0.05 mW and 0.06 mW writing optical power (which corresponds to 0.237 and 0.284 TW cm^{-2} per pulse for the amplified laser system, see Figure S1, Supporting Information) at a constant speed, respectively. The two lenses are on the same substrate at a distance of 1 mm from each other, see their optical images in Figure 2b. The setup used for the determination of their focal length is shown in Figure 2c, which consists of a spectrally filtered supercontinuum collimated laser source with $\approx 1.5 \text{ mm}$ diameter impinging at normal incidence and centered on the micro-lens under characterization. The sample is mounted on a translation stage and the transverse intensity distribution at a distance Z from the lens is recorded using a microscope objective lens and an InGaAs camera. The on-axis intensity value, taken as the maximal intensity of the recorded images, is then collected as a function of Z , as illustrated in Figure 2d at 800 nm wavelength. The latter on-axis intensity peaks at $Z = f$, where f refers to the focal length of the lens, from which the value of the refractive index n can be extracted by using the ray optics thin-lens approximation relationship $f = R/(n - 1)$, where $R = H/2 + D^2/(8H) = 65 \mu\text{m}$ is the radius of curvature of the lens, see Figure 2e. The experiment is performed in the visible and near-infrared domains, from $\lambda = 450$ to 1550 nm. This allows retrieving the refractive index dispersion, as shown in Figure 2f where the solid curves refer to the adjustment with the Cauchy law $n = A + B/\lambda^2 + C/\lambda^4$. Despite substantial variability of the retrieved refractive index (especially for the high dose lens), these results quantitatively demonstrate that 3D laser printing can be used to fabricate free-form micro-optics

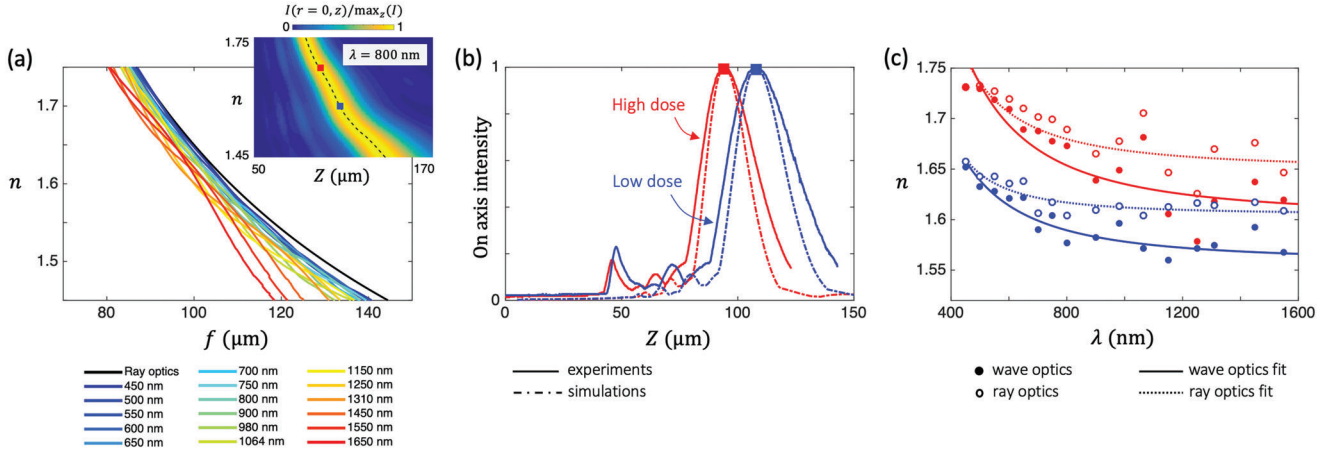


Figure 3. Wave optics approach to the assessment of refractive index. a) Simulated relationship between the focal length f and the refractive index n using wave optics propagation, see text for details. The results are shown from 450 to 1650 nm (color coded) and the ray optics expectation is added in black color (upper curve). Inset: normalized on-intensity map as a function of the refractive index at $\lambda = 800$ nm. The dashed line refers to the location of the focal plane, $Z = f$ vs n , while the two markers refer to the situation displayed in panel (b). b) Normalized on-axis intensity distribution along the propagation axis z at 800 nm wavelength for low (blue color) and high (red color) doses. Experiments: solid curves, which correspond to the data shown in Figure 2d. Simulations: dash-dotted curves. c) Retrieved refractive index dispersion from the visible to the near-infrared domain according to the protocol summarized by panels (a,b). Markers: experimental data. Curves: Cauchy fits. The data and fit obtained from the ray optics approach and shown in Figure 2f are also displayed here in order to appreciate the obtained differences.

whose optical function can be tuned by refractive index control, directly at the level of the 3D writing process. The obtained refractive index based on focusing of the micro-lenses with dimensions $< 100 \mu\text{m}$ is valuable data for the characterization of their expected performance at such scales. Still, it can be argued that the present ray optics approach has inherent limitations when dealing with micro-optics whose transverse dimensions are only a few tens of times larger than the wavelength. This is addressed in the next section where wave optics assessment is discussed.

2.3. Refractive Index Assessment: Wave Optics Approach

The wave nature of light is now accounted by simulating the actual expected transverse intensity distribution accounting for the spatially extended illumination, as depicted in Figure 1c. The calculations are made by using scalar beam propagation method based on 2D fast Fourier transform. Namely, omitting the time oscillating phase factor $\exp(-i\omega t)$, the transverse electric field amplitude at $z = Z$ is evaluated from the field at $z = H$ neglecting the diffraction between $z = 0$ and $Z = H$, according to $E(x, y, Z > H) = \mathcal{F}^{-1}\{\exp[ik_z(Z - H)]\mathcal{F}[E(x, y, H)]\}$. Here, \mathcal{F} (resp. \mathcal{F}^{-1}) refers to 2D (resp. inverse) Fourier transform, $\exp(ik_z Z)$ is the complex propagation operator in the Fourier domain with $k_z = (k^2 - k_x^2 - k_y^2)^{1/2}$, $k = \sqrt{k_x^2 + k_y^2 + k_z^2} = 2\pi/\lambda$. Assuming uniform incident illumination, we thus take $E(x, y, H) = \exp[i\Phi(x, y)]$ with $\Phi = ik[nH + (1 - n)(R - \sqrt{R^2 - r^2})]$ and $\Phi = ikH$ for $r > D/2$ with $r = \sqrt{x^2 + y^2}$. The relationship between the focal plane and the refractive index now depends on wavelength, as shown in Figure 3a, in contrast to the ray optics approach. On the one hand, the convergence of wave optics to ray optics as the wavelength decreases is retrieved, as seen in Figure 3a. On the other hand, the latter plot highlights how wave

optics can be necessary when assessing experimentally the optical properties of micro-optical elements. Indeed, in the present situation the diffraction of light from the periphery of the lens a priori also contributes to the location of the maximal on-axis intensity, which is used to define the focal length, recalling that the illumination light is plane-wave-like. Wave optics simulations also allow retrieving on-axis intensity oscillations as a function of the propagation distance as observed experimentally, as shown in Figure 3b for $\lambda = 800$ nm. This is done by calculating $I(r = 0, Z) \propto |E(0, 0, Z)|^2$ using the refractive index value that gives the maximal intensity at the same Z as in the experiments. Re-analyzing the previously introduced experimental data taken over the visible and near-infrared domain, we obtain the renewed dispersion curves displayed in Figure 3c, whose trend is to exhibit lower refractive indices than the values inferred from ray optics. Such a refined analysis leads us to similar conclusions as in the previous section regarding the unambiguous demonstration of refractive index control by adjusting the laser power used for exposure dosage.

2.4. Micro-Lenses: Optical Resolution Analysis

The optical performance of the micro-lenses fabricated with low and high doses whose refractive index has been characterized in the previous sections is analyzed through a contrast study summarized in Figure 4. The study is made by imaging a negative 1951 USAF target using the fabricated micro-lenses. In practice, the USAF target is brought as close as possible to the lens while safely ensuring non-contact with the micro-lenses in order to prevent damaging them during mutual alignment, which corresponds to a sub-mm distance that remains larger than the focal length of the micro-lens. Then, the image of a group of elements is reimaged using a $20\times$ microscope objective with 0.25

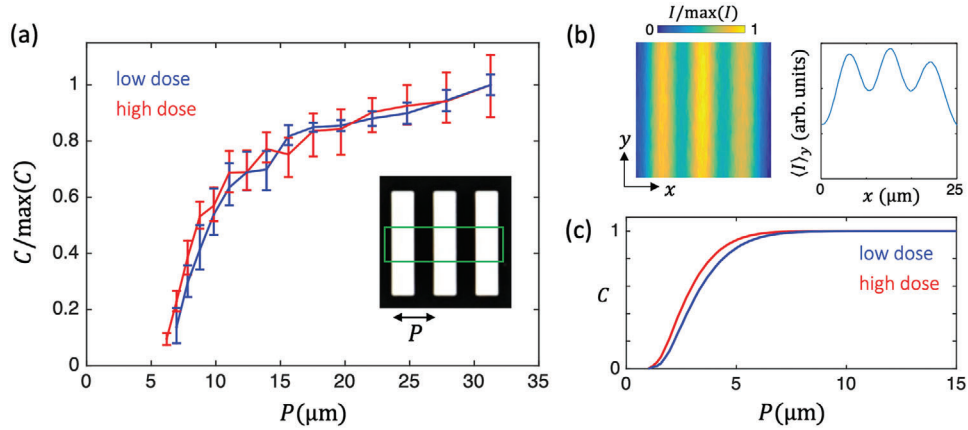


Figure 4. a) Experimental contrast C associated with optical imaging at 532 nm wavelength of negative 1951 USAF target for the low/high dose micro-lenses. Here, P is the period of a negative 1951 USAF target, see inset. The contrast data is normalized to its own maximum for both low and high-dose micro-lenses, which corresponds to the pattern 5/1 with period $P = 31.26 \mu\text{m}$ b) Recorded image of the pattern 7/1 with period $P = 7.82 \mu\text{m}$ over the region depicted in the inset of panel (a) and its profile along the x axis after averaging along the y axis. We note that the image of the pattern 7/1 is also retrieved using a positive target. c) Simulated contrast C vs P , see text for details.

numerical aperture, at 532 nm wavelength. Then, the contrast $C = (I_{\max} - I_{\min}) / (I_{\max} + I_{\min})$ of the modulated intensity profiles along the direction perpendicular of the target lines are measured and the results are normalized to their own maximum for both low and high dose micro-lenses, see Figure 4a. Obtained results are consistent with a larger refractive index for a high dose than that of low dose micro-lens as the $C(P)$ data drops at lower P for a larger dose. Indeed, a larger refractive index at fixed micro-lens geometry implies a larger numerical aperture, hence better optical resolution. Still the results are not strikingly distinguishable within the experimental error bars. Such results can nevertheless be compared to the calculated contrast of the intensity profiles of step profiles convoluted with a Gaussian beam. This is done by assuming a diffraction-limited Gaussian beam with waist radius w at $\exp(-2)$ equal to $w = 0.61\lambda/\text{NA}$ where we use the expression $\text{NA} = (D/2)/f$ for the numerical aperture and the ray optics expression $f = R/(n - 1)$ for the focal length, using $n \approx 1.63$ (low dose) and $n \approx 1.72$ (high dose) taken from the Cauchy dispersion fits obtained from the wave optics focusing experiments. The results are shown in Figure 4c, whose comparison with Figure 4a only offers a qualitative agreement. Here we recall our experimental limitation in terms of the minimal approaching distance described above, which prevents us to reach the inherent optical resolution limit of the micro-lenses. Still, this highlights another way to assess how the refractive index control implies the fine-tuning of the optical performances.

3. Discussion

Multi-photon lithography technique has been widely used for the fabrication of micro-elements for optical applications, for which it happens that the knowledge of the refractive index of the material is of paramount importance as it usually directly defines the sought-after optical function. Therefore, its post-fabrication measurement naturally appeared necessary, which has been achieved by using various techniques. However, such an approach is so far limited to 2D structures like thin films or bulky volumes of dimensions much larger than the wavelength of the employed

light. Here we prove how refractive index can be controlled directly at the fabrication step and can be exploited for free-form micro-optical elements, using micro-lenses as a prototypical example for which ray optics and wave optics refractive index measurements have been reported both in the visible and near-infrared domains.

It is worth noting that our results support the idea that the multi-photon lithography applying tight focusing and ultrashort pulses induces a significantly higher refractive index with respect to UV polymerization and can be finely adjusted by controlling the exposure dose within the dynamic fabrication window over a range than leads to readily observable changes of the optical function encoded in the 3D shape. Further optimization studies taking into account exact voxel dimensions' dynamics corresponding to its spatial overlap^[28] or specially engineered materials could lead to an even higher range of achievable refractive index values. This is essential for the active micro-optics, where the exact refractive index for the pump and emission wavelengths is critical and must be considered designing the micro-laser cavities.^[29]

This opens the possibility of the design and fabrication of 4D printing (freedom in 3D shape and on-demand refractive index) of free-form micro-optical elements and stacked components out of a single hybrid organic-inorganic pre-polymer material. That is offering next step for free-form morphology and inhomogeneous refractive index distribution. Further work is foreseen for establishing a standardized light-induced damage threshold (LIDT) measurement protocol for specifically volumetric micro-optical components having a high surface-to-volume aspect ratios^[30] and studying a laser writing induced birefringence.^[23]

It was validated that the refractive index control can be achieved using low and high exposure doses by both laser oscillator and amplifier-based systems reaching applied intensities at the specimen within the range of 0.237 and 0.284 TW cm^{-2} . This makes the findings applicable independently of the specific pulsed exposure source and is compatible with the commercially available workstations as well as custom-built setups.

4. Experimental Section

Chemicals and Materials: Hybrid organic–inorganic photopolymer SZ2080 provided by Prof. Maria Farsari Lab. Oil immersion Immersol 518 with $n_{oil} = 1.518$ (23°C). Cargille immersion oils worked as the refractive index fluids with tabulated and well-reported dispersion relation and refractive index from 1.4 to 1.596 with a step of 0.004 refractive index value.

Sample Preparation and Development: An hybrid organic–inorganic photoresin SZ2080, with reported refractive index of $n_{SZ2080} = 1.52$ at 589.3 nm,^[31] was photosensitized with 1 wt% concentration of Irgacure 369 (2-benzyl-2-(dimethylamino)-4'-morpholinobutyrophenone) to enhance the polymerization reaction.^[32] The sol–gel photopolymer was drop-casted on a glass coverslip ($n_{glass} = 1.52$, thickness of 130–170 μm) and gradually dried on a hot plate. After fabrication, the sample was immersed in 4-methyl-2-pentanone (MIBK) to wash out non-polymerized material.

Micro-Optics Design: Spherical micro-lenses were design for an specific f , R , and D . The 3D geometry of the lenses was fabricated with concentric circles as a writing method. The micro-lens was sliced into different layers in height to ensure the spherical shape of the lens, and for each layer, concentric circles were written by the laser beam. The micro-lenses were designed to be of $R = 65$ and $D = 50$ μm .

UV Polymerization: A droplet of SZ2080 photopolymer was drop-casted on a glass coverslip and was illuminated with UV light for around 30 min.

Laser Direct Writing System Based on Laser Oscillator: Fabrication of micro-structures performed on Laser Nanofactory system from Femtika. Femtosecond laser beam with a second harmonic at $\lambda_{sh} = 517 \pm 10\text{nm}$ with 144 fs pulse duration and 76 MHz pulse repetition rate. The positioning system of linear stages with an accuracy of ± 300 nm in the XY axis and ± 270 nm in the Z axis. Galvano scanners are used for laser beam positioning with an accuracy of 50 μrad and feedback resolution of 0.007 μrad . The fabrication process is monitored by an integrated vision system and it is controlled by 3DPoli software. A Plan Achromat Zeiss 63x, 1.4 NA immersion oil objective lens is used to focus the laser beam in the photopolymer. An oil immersion is used between the specimen and the microscope objective. The micro-lenses were fabricated with laser power of 2 and 4 mW that stand for Low dose and High dose, respectively, corresponding to 0.21 and 0.42 TW cm^{-2} .

Laser Direct Writing System Based on Amplified Laser: Fabrication performed on custom-made setup adapted from FemtoLAB. Femtosecond beam from Yb:KGW laser (Pharos, Light Conversion, Co., Ltd) with second harmonic $\lambda_{sh} = 515$ nm, with 300 fs pulse duration and, 200 kHz repetition rate. The fabrication process is monitored by an integrated vision system and it is controlled by 3DPoli software. A Plan Achromat Zeiss 63x, 1.4 NA immersion oil objective lens is used to focus the laser beam in the photopolymer. An oil immersion is used between the specimen and the microscope objective. The micro-lenses were fabricated with laser power of 0.05 and 0.06 mW that stands for Low dose and High dose, respectively, corresponding to 0.237 and 0.284 TW cm^{-2} .

Scanning Electron Microscopy: An SEM Thermo Scientific Quanta 250 (Agawam, MA, USA), was used for the topological characterization of the micro-elements. Secondary electrons were used to image the sample covered with a thin Ag layer of around 10 nm.

Index-Matching Measurements: Supercontinuum laser for illumination from vis to IR (350–1750 nm) SuperK EXU, filtered for 17 different frequencies (450, 500, 550, 600, 650, 700, 750, 800, 900, 980, 1064, 1150, 1250, 1310, 1450, 1550, and 1650 nm). Two linear polarizers control the intensity of the incident light on the sample. Light collected by a 20x microscope objective and a CCD camera.

Focal Length Measurements: Supercontinuum laser for illumination from vis to IR (350–1750 nm) SuperK EXU, filtered for 17 different frequencies (450, 500, 550, 600, 650, 700, 750, 800, 900, 980, 1064, 1150, 1250, 1310, 1450, 1550, and 1650 nm). The sample is placed on a translation stage for the displacement of the imaging plane along the laser beam axis. An imaging system of a microscope objective and a CCD camera to collect the intensity at the focal point of the micro-lenses.

Optical Imaging: The optical performance of the micro-lenses was characterized by imaging a Target unit (Thorlabs R3L1S4P and R1DS1N - Positive and Negative 1951 USAF targets were used and indicated were appropriate) in an optical microscope (Olympus BX51) with a 40x microscope objective. The target unit was placed at infinity, that is, at some distance from the micro-lenses, and illuminated with white light.

Acknowledgements

The authors were deeply thankful to VU LRC colleagues Ph.D. students Simonas Varapnickas and Edvinas Skliutas for assisting with the fabrication of the micro-optical components and their characterization with high-resolution SEM imaging, respectively. D.G-H's present address is King Abdullah University of Science and Technology (KAUST), Thuwal, Saudi Arabia, and the described research was part of her master thesis project as Europhotonics (International Master in Photonics program) scholarship.

Funding Information

This work received financial support from EU Horizon 2020, Research and Innovation program LASERLAB-EUROPE JRA project no. 871124 (M.M.), from the European Social Fund (project no. 09.3.3-LMT-K712-17-0016) under the grant agreement with the Research Council of Lithuania (LMTLT) (D.G.), and from the Initiative of Excellence of the University of Bordeaux program, grant agreement ANR-10-IDEX-03-02 (B.S-P., S.J. and E.B.).

Conflict of Interest

The authors declare no conflict of interest.

Data Availability Statement

The data that support the findings of this study are available in the supplementary material of this article.

Keywords

3D micro-optics, 4D printing, index matching, laser 3D nanolithography, optical 3D printing, refractive index, SZ2080

- [1] L. Yang, F. Mayer, U. Bunz, E. Blasco, M. Wegener, *Light Adv. Manuf.* **2021**, 2, 296.
- [2] M. Bouzin, A. Zeynali, M. Marini, L. Sironi, R. Scodellaro, L. D'Alfonso, M. Collini, G. Chirico, *Sensors* **2021**, 21, 5891.
- [3] D. Gonzalez-Hernandez, S. Varapnickas, A. Bertoincini, C. Liberale, M. Malinauskas, *Adv. Opt. Matter.* **2022**, 11, 2201701.
- [4] S. Varapnickas, S. Chandran Thodika, F. Moroté, S. Juodkazis, M. Malinauskas, E. Brasselet, *Appl. Phys. Lett.* **2021**, 118, 151104.

- [5] H. Yu, Q. Zhang, B. P. Cumming, E. Goi, J. H. Cole, H. Luan, X. Chen, M. Gu, *Adv. Sci.* **2021**, *8*, 2100141.
- [6] A. Toulouse, J. Drozella, P. Motzfeld, N. Fahrbach, V. Aslani, S. Thiele, H. Giessen, A. Herkommer, *Opt. Express* **2022**, *30*, 707.
- [7] I. V. A. K. Reddy, A. Bertocini, C. Liberale, *Optica* **2022**, *9*, 645.
- [8] G. Merkininkaitė, E. Aleksandravičius, M. Malinauskas, D. Gailevičius, S. Šakirzanovas, *Opto-Electr. Adv.* **2022**, *5*, 210077.
- [9] D. Gonzalez-Hernandez, S. Varapnickas, G. Merkininkaitė, A. Čiburys, D. Gailevičius, S. Šakirzanovas, S. Juodkazis, M. Malinauskas, *Photonics* **2021**, *8*, 577.
- [10] M. Schmid, A. Toulouse, S. Thiele, S. Mangold, A. Herkommer, H. Giessen, *Adv. Funct. Mater.* **2022**, <https://doi.org/10.1002/adfm.202211159>.
- [11] S. Dottermusch, D. Busko, M. Langenhorst, U. Paetzold, B. Richards, *Opt. Lett.* **2019**, *44*, 29.
- [12] M. Schmid, D. Ludescher, H. Giessen, *Opt. Mater. Express* **2019**, *9*, 4564.
- [13] L. Pertoldi, V. Zega, C. Comi, R. Osellame, *J. Appl. Phys.* **2020**, *128*, 175102.
- [14] E. Kabouraki, V. Melissinaki, A. Yadav, A. Melninkaitis, K. Tourlouki, T. Tachtsidis, N. Kehagias, G. D. Barmparis, D. G. Papazoglou, E. Rafailov, M. Farsari, *Nanophotonics* **2021**, *10*, 3759.
- [15] L. J. Jiang, Y. S. Zhou, W. Xiong, Y. Gao, X. Huang, L. Jiang, T. Baldacchini, J.-F. Silvain, Y. F. Lu, *Opt. Lett.* **2014**, *39*, 3034.
- [16] A. Žukauskas, I. Matulaitienė, D. Paipulas, G. Niaura, M. Malinauskas, R. Gadonas, *Laser Photon. Rev.* **2015**, *9*, 706.
- [17] J. Qu, M. Kadic, A. Naber, M. Wegener, *Sci. Rep.* **2017**, *7*, 40643.
- [18] C. R. Ocier, C. A. Richards, D. A. Bacon-Brown, Q. Ding, R. Kumar, T. J. Garcia, J. van de Groep, J.-H. Song, A. J. Cyphersmith, A. Rhode, A. N. Perry, A. J. Littlefield, J. Zhu, D. Xie, H. Gao, J. F. Messinger, M. L. Brongersma, K. C. T. Jr, L. L. Goddard, P. V. Braun, *Light Sci. Appl.* **2020**, *9*, 196.
- [19] X. Porte, N. Dinc, J. Moughames, G. Panusa, C. Juliano, M. Kadic, C. Moser, D. Brunner, D. Psaltis, *Optica* **2021**, *8*, 1281.
- [20] J.-S. Boisvert, A. Hlil, S. Loranger, A. Riaz, Y. Ledemi, Y. Messadeq, R. Kashyap, *Sci. Rep.* **2022**, *12*, 1323.
- [21] A. Grabulosa, J. Moughames, X. Porte, D. Brunner, *Nanophotonics* **2022**, *11*, 1591.
- [22] M. Ziemczonok, A. Kus, P. Wasylczyk, M. Kujawinska, *Sci. Rep.* **2019**, *9*, 18872.
- [23] M. Schmid, H. Giessen, *Opt. Lett.* **2022**, *47*, 5789.
- [24] A. Ovsianikov, J. Viertl, B. Chichkov, M. Oubaha, B. MacCraith, I. Sakellari, A. Giakoumaki, D. Gray, M. Vamvakaki, M. Farsari, C. Fotakis, *ACS Nano* **2008**, *2*, 2257.
- [25] A. Žukauskas, G. Batavičiūtė, M. Ščiuka, Z. Balevičius, A. Melninkaitis, M. Malinauskas, *Opt. Mater.* **2015**, *39*, 224.
- [26] B. Liu, B. Dong, C. Xin, C. Chen, L. Zhang, D. Wang, Y. Hu, J. Li, L. Zhang, D. Wu, J. Chu, *Small* **2022**, *19*, 2204630.
- [27] D. Samsonas, E. Skliutas, A. Čiburys, L. Kontenis, D. Gailevičius, J. Berzins, D. Narbutis, V. Jukna, M. Vengris, S. Juodkazis, M. Malinauskas, *Nanophotonics* **2023**, <https://doi.org/10.1515/nanoph-2022-0629>.
- [28] T. F. Scott, C. J. Kloxin, D. L. Forman, R. R. McLeod, C. N. Bowman, *J. Mater. Chem.* **2011**, *21*, 14150.
- [29] H. M. R. de la Cruz, E. Ortiz-Ricardo, V. A. Camarena-Chavez, A. Martinez-Borquez, G. Gutierrez-Juarez, A. B. U'Ren, R. Castro-Beltran, *Appl. Opt.* **2021**, *60*, 720.
- [30] A. Butkutė, L. Čekanavičius, G. Rimšelis, D. Gailevičius, V. Mizeikis, A. Melninkaitis, T. Baldacchini, L. Jonušauskas, M. Malinauskas, *Opt. Lett.* **2020**, *45*, 13.
- [31] V. Melissinaki, M. Farsari, S. Pissadakis, *Fibers* **2017**, *5*, 1.
- [32] E. Skliutas, M. Lebedevaite, E. Kabouraki, T. Baldacchini, J. Ostrauskaite, M. Vamvakaki, M. Farsari, S. Juodkazis, M. Malinauskas, *Nanophotonics* **2021**, *10*, 1211.